Air sensitivity of MoS_2, $MoSe_2$, $MoTe_2$, HfS_2 and $HfSe_2$

Gioele Mirabelli,[1] Conor McGeough,[2] Michael Schmidt,[1] Eoin K. McCarthy,[3] Scott Monaghan,[1] Ian M. Povey,[1] Melissa McCarthy,[1] Farzan Gity,[1] Roger Nagle,[1] Greg Hughes,[2] Attilio Cafolla,[2] Paul K. Hurley,[1] Ray Duffy[1]

[1]Tyndall National Institute, University College Cork, Cork, Ireland. [2]School of Physical Sciences, Dublin City University, Dublin 9, Ireland. [3]Advanced Microscopy Laboratory, Trinity College Dublin, Dublin, Ireland.

ABSTRACT : A surface sensitivity study was performed on different transition-metal dichalcogenides (TMDs) under ambient conditions in order to understand which material is the most suitable for future device applications. Initially, an Atomic Force Microscopy (AFM) and Scanning Electron Microscopy (SEM) study was carried out over a period of 27 days on mechanically exfoliated flakes of 5 different TMDs, namely MoS_2, $MoSe_2$, $MoTe_2$, HfS_2 and $HfSe_2$. The most reactive were $MoTe_2$ and $HfSe_2$. $HfSe_2$ in particular showed surface protrusions after ambient exposure reaching a height and width of approximately 60 nm after a single day. This study was later supplemented by Transmission Electron Microscopy (TEM) cross-sectional analysis, which showed hemispeherical-shaped surface blisters that are amorphous in nature approximately 180-240 nm tall and 420-540 nm wide, after 5 months of air exposure, as well as surface deformation in regions between these structures, related to surface oxidation. An X-ray photoelectron spectroscopy (XPS) study of atmosphere exposed $HfSe_2$ was conducted over various time scales which indicated the Hf undergoes preferential reaction with oxygen as compared to the Se. Energy-Dispersive X-Ray Spectroscopy (EDX) showed that the blisters are Se-rich, thus it is theorised that HfO_2 forms when the $HfSe_2$ reacts in ambient, which in turn causes the Se atoms to be aggregated at the surface in the form of blisters. Overall it is evident that air contact drastically affects the structural properties of TMD materials. This issue poses one of the biggest challenges for future TMD-based devices and technologies.

INTRODUCTION

Silicon is a relatively stable material, mechanically strong, with a reliable thermal oxide. These reasons have contributed to the popularity of silicon for advanced semiconductor integrated circuits over the past number of decades. However, for many reasons alternate semiconductors with high carrier mobilities, are being considered as channel materials for future electronic devices.

As well as electronic or optoelectronic properties, the ease of handling, fabrication, and manufacturability of semiconductor materials are key issues in order for a material to progress from the research lab to the large-scale production environment. Transition metal dichalcogenides (TMDs) have shown potential, but their practicality remains an open question. Can they be fabricated reliably over large areas? Can they be integrated to the same levels of complexity as silicon has been to date? One of these open issues is the air sensitivity of TMD materials. How quickly do they degrade and what form do the resulting species take? Do these features limit practical future use? In this study we explore surface stability of MoS_2, $MoSe_2$, $MoTe_2$, HfS_2 and $HfSe_2$ in terms of surface roughness, surface terminations, oxide homogeneity, and we highlight possible future integration schemes.

The sensitivity of TMDs to oxygen and water molecules after air exposure has been reported before, showing a reduction of the on-state current in Field Effect Transistor (FET) devices by up to 2 orders of magnitude, [1] work function changes, [2] an instability of the Fermi level position,[3] and an increase in material resistivity.[4] In many cases an annealing cycle resulted in the desorption of surface molecules and therefore improved the device characteristics. The drastic change in the electrical performance of TMD devices was also studied by Park et al.,[5] where the electrical current dropped significantly after air exposure. In order to limit such effects a resist-based passivation of the surface was applied. Thus, even if deterioration due to air exposure was shown in some publications, [6,7] to our knowledge a

systematic experimental study on the effects and reactions of the surface of TMDs when exposed to the ambient is lacking.

In this article we report a systematic study of MoS_2, $MoSe_2$, $MoTe_2$, HfS_2 and $HfSe_2$ surfaces in air. First an AFM study over a period of 27 days was carried out to understand the main differences between each TMD in terms of sensitivity upon air exposure. The results of this study were then confirmed by SEM measurements. An XRD study of $HfSe_2$, the most reactive TMD in this study, was performed to provide a quantitative insight on the reactions of the material. XPS measurements were used to determine the surface chemical composition and to investigate changes in the chemical state of the surface with ambient exposure. By observing the binding energy shifts and broadening of the core level peaks the extent of surface oxidation can be inferred. Furthermore, TEM cross-sections and EDX analysis give a better understanding of the structure of the surface features.

EXPERIMENTAL

All of the TMD considered were synthetic, except for MoS_2 which was natural. For each of them, flakes were mechanically exfoliated from their bulk crystal counterpart using the classic Scotch tape technique.[8] Then, the flakes on the tape were gently pressed on a substrate composed of 85 nm of SiO_2 on a highly-doped Si handle wafer. Immediately after the exfoliation, without applying any method to clean the TMD surface, the samples were examined by AFM for an initial comparison of the materials under study. The AFM was operated in Tapping-Mode in order to avoid any alteration of the surface due to the contact between the AFM tip and the surface itself. For each sample, every effort was made to repeatedly measure the same flake at approximately the same location, over an area of 5×5 μm^2. In the AFM study, the same analysis was systematically carried out periodically on each material over a 27 day period. Root-mean-square (RMS) roughness evolution of the surfaces

gave an important comparison to understand the main differences between the TMDs studied, considering both a change of the metal (Mo or Hf) and/or a change of the chalcogen element (S, Se or Te).

The morphologies of the TMD sample surfaces were investigated using a FEI Quanta 650 SEM in high-vacuum. In order to improve the imaging of the samples gold was sputtered using an Agar sputter-coater. For structural analysis, cross-section samples were obtained by using the Dual Beam Helios Nanolab 600i system from FEI, using a Ga ion beam. Layers of protective material were used consisting of electron beam deposited C, Pt, and ion beam deposited C. Lamellas were thinned and polished at 30 kV 100 pA and 5 kV 47 pA, respectively. Cross-sectional Transmission Electron Microscopy (XTEM) imaging was carried out using a JEOL 2100 HRTEM operated at 200 kV in bright field mode using a Gatan Double Tilt holder. EDX analysis was performed using STEM-EDX on a FEI Titan 80-300kV S/TEM. Analytical STEM provides a sub-nanometre, high current probe (~0.5 nm, 0.56 nA) allowing for site specific EDX analysis on the nanometre scale.

For the XPS analysis flakes were mounted and held on an XPS sample holder using an adhesive carbon pad. Flakes were then cleaved using the Scotch tape method and placed into a vacuum chamber in less than 30 seconds to minimise atmospheric contamination for the base, freshly cleaved, measurement. Once the freshly cleaved flake was measured the sample was removed and exposed to ambient atmospheric conditions for a period of 1 hour and reloaded for XPS measurement. The process of exposing the sample was repeated for a 3 hour and a 48 hour exposure. Following the 48 hour measurement the flake was re-cleaved using Scotch tape. For $HfSe_2$ the XPS spectra were taken of the Hf 4f and the Se 3d core level peaks following the different exposure times to observe how the peaks shapes change and more importantly the relationship of the ratio of the area under each peak which directly reflects the relative concentrations of the elements present within the XPS sampling depth

which is typically 5-7 nm. The XPS system used an aluminium anode to generate X-ray photons of 1486 eV and had an operating base pressure of approximately 2.0×10^{-9} mbar with the analysis area of the order of 0.5 cm^2.

RESULTS

In Figs. 1 and 2 are representative AFM images of MoS_2 and $HfSe_2$ surfaces 24 hours after exfoliation. These two materials were the most stable and least stable extremes respectively, of the TMDs studied. Twenty four hours after exfoliation, $HfSe_2$ showed clear signs of degradation. Its surface, as shown in Fig. 2, is characterised by several protrusions randomly located across the surface. The tallest of these was found to be 57.4 nm high after 1 day, as is clear from the cross-section in the inset of Fig. 2. This ambient exposure behaviour is in clear contrast to that observed for MoS_2. The 2D AFM image in Fig. 1 shows a darker z-shaped region. A cross-sections analysis shows this feature to be approximately 0.65 nm deep , which suggests a missing single-layer of MoS_2, which is known to be ~0.65 nm thick. This might be related to the stress induced on the surface through the mechanical exfoliation process. The same feature was located in later AFM measurements and there were no signs of any deterioration, meaning that even 27 days after exfoliation the material is relatively stable upon air exposure.

The overall results of the AFM study can be summarised by the RMS roughness trends of the surfaces shown in Fig. 3, for both the Mo-based and Hf-based TMDs. As previously stated, the MoS_2 surface showed the best stability and it is the only TMD that did not show any noticeable additional visible features or surface change during the period of study, implying that it is the most suitable TMD for electronic applications from a material point of view. The RMS roughness values for MoS_2 are comparatively low (~0.2-0.4 nm) and approximately constant throughout the 27 days. $MoSe_2$ showed one peak related to air

exposure, similar to those found on $HfSe_2$ surface, of ~27 nm height on the 9th day after exfoliation. Subsequently, on the 27th day, the surface was quite degraded, but without any other tall protrusions. $MoTe_2$ surface features were detectable after 3 days and were spread almost uniformly across the surface. These studies indicate a general trend in decreasing ambient stability for a given metal in the TMD as the chalcogen element changes from S to Se and finally Te. For example, from Fig. 3(a) it is seen that the RMS roughness of HfS_2 is significantly lower than that of $HfSe_2$ during the period studied. The degradation of $HfSe_2$ is visible 1 day after exfoliation, while signs of degradation are only visible 9 days after exfoliation for HfS_2.

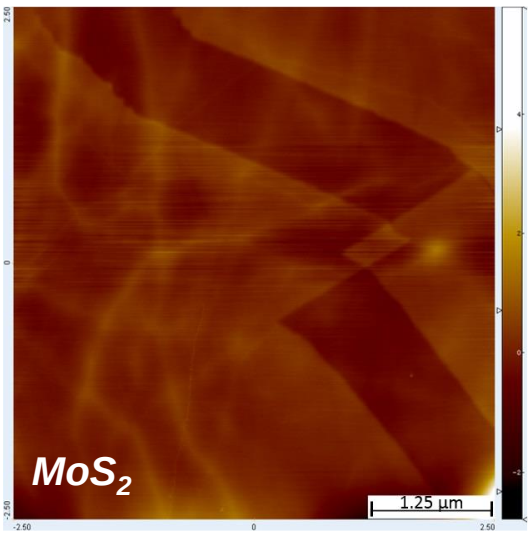

Figure 1 : Representative MoS_2 AFM image taken 24 hours after exfoliation.

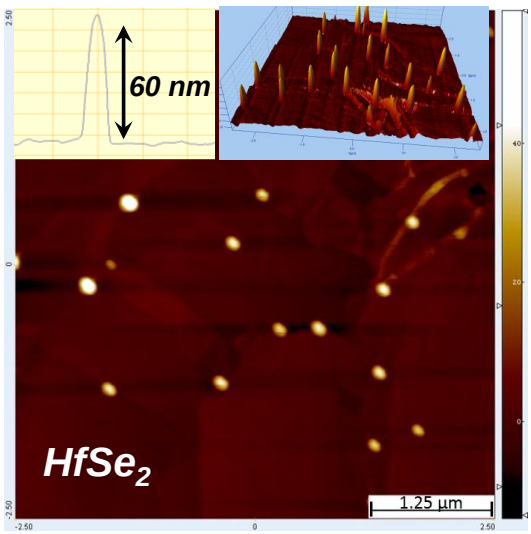

Figure 2 : Representative $HfSe_2$ AFM image taken 24 hours after exfoliation. The insets show cross-section of the tallest protrusion found on $HfSe_2$ of approximately 60 nm, and a 3D representation of the data.

Some variation is noted in the RMS data shown in Fig. 3 which may be attributed to a number of factors; while it was attempted to return to the exact same 5 µm × 5 µm area on each flake, there may have been some misalignment due to handling or variation caused by changing AFM tip over the period of study. Furthermore, for the $HfSe_2$ it was noted that some of the surface features disappeared from one measurement to the next, which may indicate that these features are not tightly bound to the surface. Despite this "noise" in the

data in Fig. 3, the overall trends observed are reliable, namely a general surface roughening with time, with observable differences between the five TMDs under study.

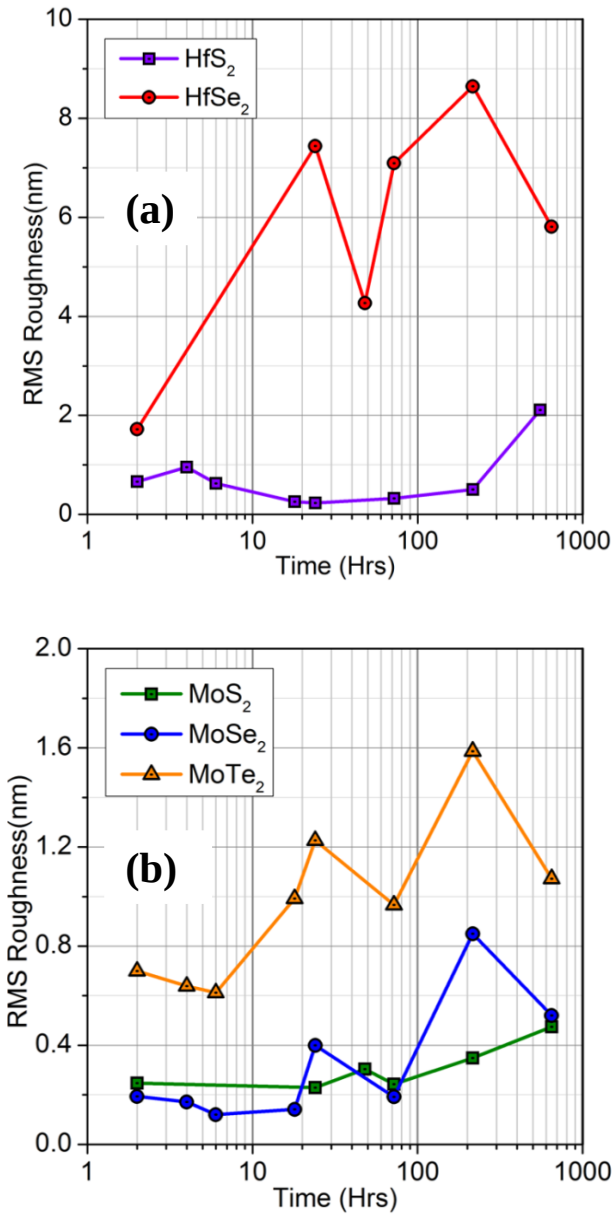

Figure 3 : RMS surface roughness trends for (a) Hf-based and (b) Mo-based TMDs. Note the difference in the y-axis scales.

In order to analyse the results of the AFM study more thoroughly, all TMDs were examined by SEM, and $HfSe_2$ was further studied by STEM, XTEM, EDX, and XPS, since it showed the highest reactivity on contact with air. By analysing the behaviour of the most reactive TMD we hoped to address the most volatile material system.

Fig. 4(a) shows an SEM measurement of the $HfSe_2$ surface five months after exfoliation. The measurement was delayed for this period of time in order to get a clear picture of the surface blisters. The inset shows the surface 1 day after exfoliation, which shows the same kind of blister like protrusions in terms of form and shape, only smaller. Furthermore, it is clear from the images that the blisters have a higher density at the step-edges. The step-edges of the top-surface, related to the mechanical exfoliation method, are characterised by dangling bonds that may be optimal nucleation sites for the growth of the features.

Also, it is important to compare the density of protrusions found during the AFM study. The blister density in the AFM image in Fig. 2, is approximately 8×10^7 cm^{-2}, while the SEM image in Fig. 4(a) has a blister density of approximately 4.3×10^7 cm^{-2}. The difference in defect density is attributed to the fact that a different area was scanned in AFM and SEM. Note, the same type of terrace edges were found on MoS_2 (Fig. 1), but they were not decorated with growths of blister-like features during the period of study. Other TMDs were studied by SEM in a similar way, but no obvious surface features were observed. For example, Fig. 4(b) shows the HfS_2 surface after 5 months of air exposure. The terraced nature of the material is obvious, and is related to the layered structure of the material itself, and the mechanical exfoliation process. The surface appears to be uniform with no blisters present, at least under this magnification. A similar lack of obvious surface features was characteristic in the SEM images of MoS_2, $MoSe_2$, and $MoTe_2$.

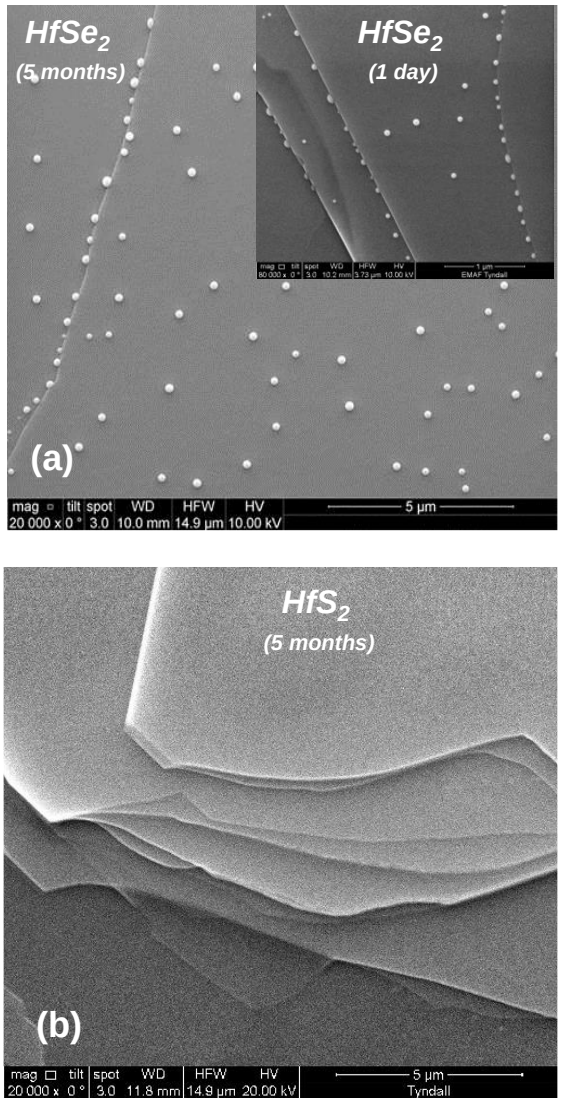

Figure 4 : (a) Representative SEM image of $HfSe_2$ 5 months from exfoliation; the inset shows the surface 1 day from exfoliation, which shows the same kind of protrusions in terms of form and shape, only smaller. (b) Representative image of HfS_2 after 5 months from exfoliation. The terracing is related to the mechanical exfoliation and the layered nature of the material. No blister features appear to be evident.

TEM cross-section analysis was carried out in order to understand the detailed structure of the features on $HfSe_2$, and their chemical composition, through EDX analysis. Fig. 5 shows representative images of $HfSe_2$ after 5 months of air exposure. In the following Figures (Figs. 5-7) the surface features look like hemispherical shaped blisters which are approximately 180-240 nm tall and 420-540 nm wide. Fig. 5(a) shows a $HfSe_2$ flake which is approximately 280 nm thick, while Fig. 5(b) is a thinner flake which is approximately 40 nm thick. Blisters appear on both thick and thin flakes with approximately the same dimensional

size. The material within the blister appears to be amorphous in nature. The blister on the right side of Fig. 5(a) is partially cut and is not entirely contained within the TEM lamella. Note the blisters are surface features, and are not formed throughout the bulk of the material. A delamination crack is evident in the same figure within the $HfSe_2$, highlighting that these TMDs are layered materials that may have mechanical weaknesses between the layers. It should be noted that the crack is likely to have occurred during TEM sample preparation.

In terms of area coverage, assuming a circular blister with average width of 480 nm, and a density of 4.3×10^7 cm^{-2}, the area covered by these features is approximately 8% of the $HfSe_2$ surface.

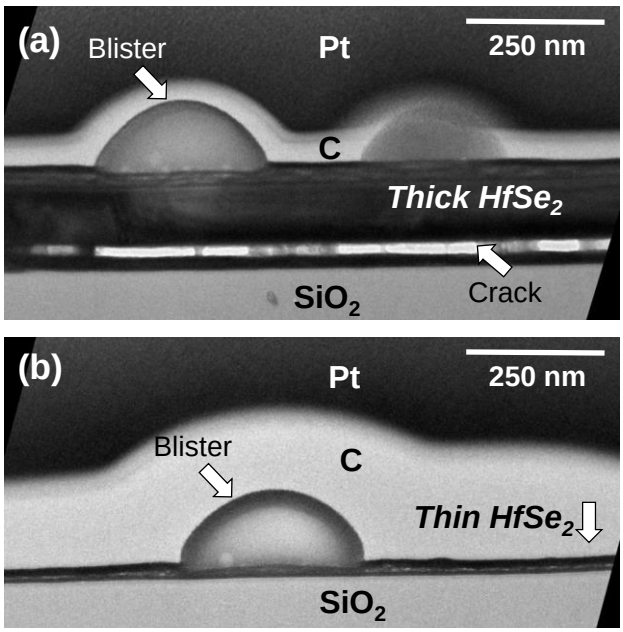

Figure 5 : Representative TEM images of $HfSe_2$ after 5 months of air exposure. Hemispherical shaped surface features appear to be amorphous in nature and are of similar dimensional size on both the (a) thick and (b) thin flakes.

Fig. 6 shows a higher magnification image of the thicker flake, as in Fig. 5(a), which shows more detail of the surface features. It appears that the surface region of the $HfSe_2$ beneath the blister is highly disordered. Also the top surface of the $HfSe_2$, between the blisters, appears to be degraded as it is non-uniform and less homogeneous than the bulk portion of the flake. Thus the surface reactions resulting from ambient exposure of $HfSe_2$

could be considered to consist of two distinct features, namely localised blisters and planar surface modification.

Fig. 7 provides extra insight into the structural makeup of the blisters, as the thinner flake, seen in Fig. 5(b) was examined further. A surface blister was magnified, and initially appeared homogeneous. However with prolonged electron irradiation over several minutes, a void appeared in the middle of the feature, as shown in Fig. 7(b). The void is likely formed by beam induced knock-on damage causing a small void to appear and proliferate to a large hole.. It may be coupled with beam induced heating causing a melting type effect. This may indicate that the middle of these features are structurally less stable, much like a bubble. Also note that the Au, deposited to enable the SEM imaging as indicated earlier, is visible on the outer surfaces of these features.

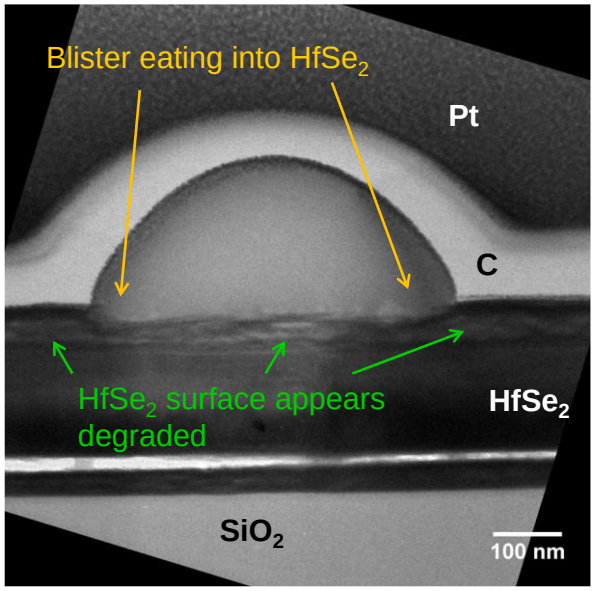

Figure 6 : Representative TEM image of the surface blisters on the thick $HfSe_2$ flake.

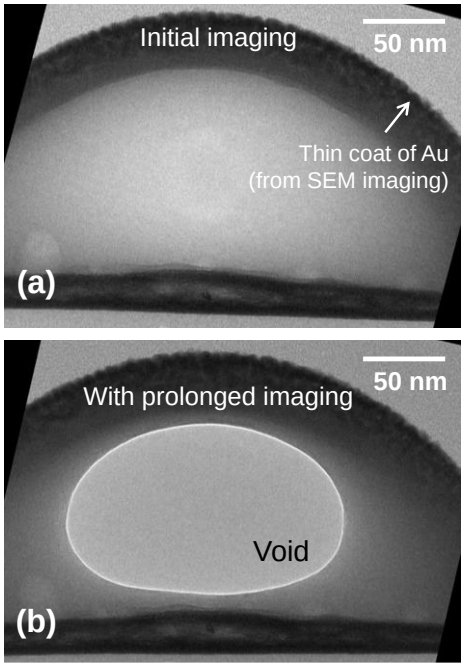

Figure 7 : TEM imaging of the blisters on the thin $HfSe_2$ flake shows that (a) during initial imaging the blister is continuous and that (b) after a few minutes of electron irradiation a void is formed in the middle..

Fig. 8 shows compositional analysis performed on the surface blisters via STEM based EDX. Fig. 8(a) shows a STEM image across which the EDX analysis was performed.

In the STEM image the contrast is reversed compared to bright field TEM. The structural non-uniformity is again evident in regions below the blister, and to the left and right of it. Figs. 8(b) and 8(c) show the EDX maps for Hf and Se respectively recorded across the STEM image in shown in Fig. 8(a). Notice that the blister is primarily composed of Se, with only trace amounts of Hf. There are patches within the $HfSe_2$ layer that show increased concentrations of Hf accompanied by a Se deficit in the same region. These Hf/Se concentration changes are only present at the top of the layer. The bulk region of the $HfSe_2$ is uniform.

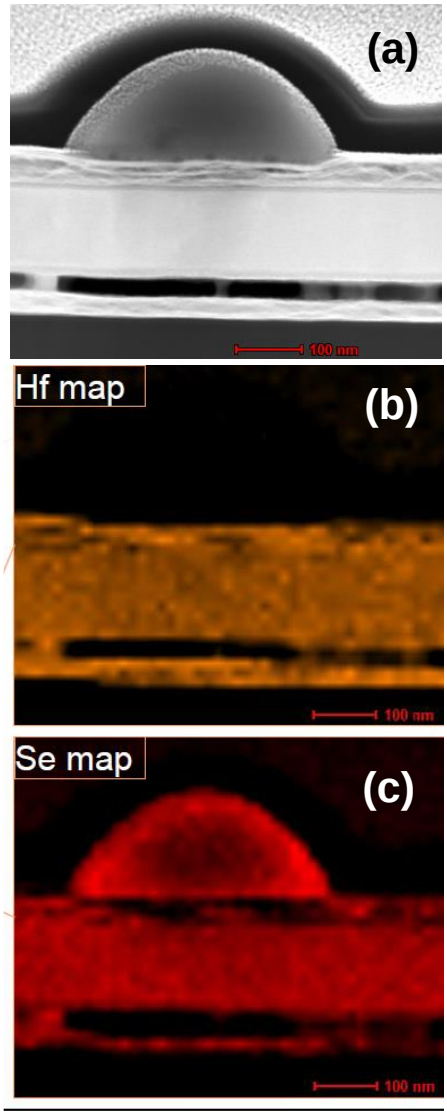

Figure 8 : EDX data showing (a) the region mapped, (b) the Hf map, and (c) the Se map within the $HfSe_2$ flake and surface blister. The blister is Se-rich with little or no Hf present. The regions below the blister are depleted of Se.

The XPS study data for $HfSe_2$ as a function of ambient exposure are displayed in Figs. 9-11. The change in the elemental stoichiometry with ambient exposure time is displayed in Figure 9 and clearly shows the progressive loss of Se from within the XPS sampling depth (5-7 nm) over the 48 hr monitoring period with the Se:Hf ratio reducing from the initial 2:1 to 1.4:1. Note a similar study on MoS_2 showed no changes in the elemental composition under an equivalent ambient exposure again confirming relative surface stability.

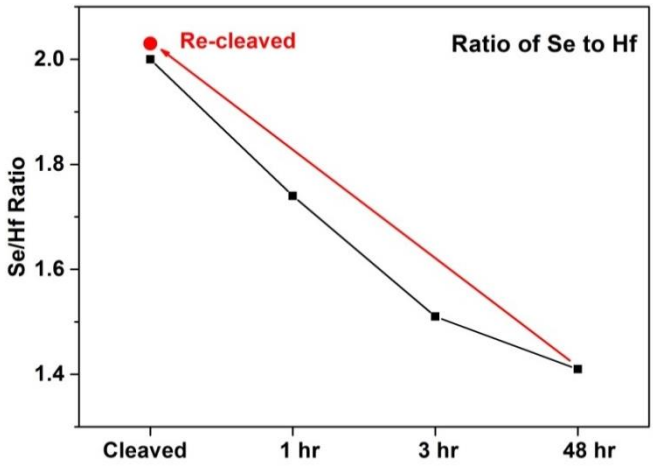

Fig 9: Plot of the change in Se/Hf elemental ratio following ambient exposure of the freshly cleaved surface. The re-cleaving process restores the surface to the original elemental composition by removal of the oxidised surface.

Analysis of the changes in the profile of the Hf 4f peak over the time span of this ambient exposure study shown in Fig. 10 indicates increasing evidence for Hf oxidation. The Hf 4f peaks from a freshly cleaved sample in Fig.10(a) have a binding energy of 14.3 eV and 16 eV for the $Hf_{7/2}$ and $Hf_{5/2}$ component peaks respectively,[9] which are indicative of a Hf signal in the $HfSe_2$ crystal. The appearance and subsequent increase in intensity of component peaks, at binding energies of 15.4 eV and 17.1 eV in Fig. 10 (b, c, and d), are indicative of the progressive oxidation of the Hf as the higher electronegativity of oxygen compared to selenium results in this core level shift.[10] The corresponding curve fitted Se 3d

spectra, [11] displayed in Fig. 11 show a broadening of the peak profile without any evidence of higher Se oxidation states. This can be interpreted in terms of the preferential formation of Hf oxides following ambient exposure with the consequential release of Se, some of which desorbs from the surface and some of which gets trapped in the blister structures. The fact that these blisters are predominantly found along step edges is consistent with the Hf oxidation process initiating along the step edges where ideal surface termination is absent.

Further evidence for the preferential oxidation of Hf over Se comes from the binding energy and FWHM of the O1s peaks. In Fig. 12, the FWHM of the 48 hrs exposed sample is 2.9 eV at 530.9 eV binding energy in agreement with Liu et al.[12] who reports a HfO_2 peak on a Si substrate to have a FWHM of 2.6 eV at a binding energy of 530.8 eV. Combined with the lack of evidence for SeO_2 in the Se3d spectra it can be concluded that the oxide is due to HfO_2.

Considering the surface area contributing to the XPS spectra is of the order of 0.5 cm^2, it is reasonable to conclude that the photoemission spectra are dominated by the areas between the blisters, which remain largely unchanged, as the surface coverage of these feature was estimated to be approximately 8%.

A remaining question is why the Se atoms produced by the preferential Hf oxidation coalesce into hemispherical features, as opposed to aligning parallel to the surface. The presence of a hemispherical shape suggests a construction to minimise surface tension. One possible explanation is that, as a result of the high temperature vapour phase growth process for the $HfSe_2$, gases are trapped between the 2D layers of the crystal, and the surface features contain a gas. This is currently being investigated using scanning Auger with a spot size resolution less than the typical diameter of the hemispherical features.

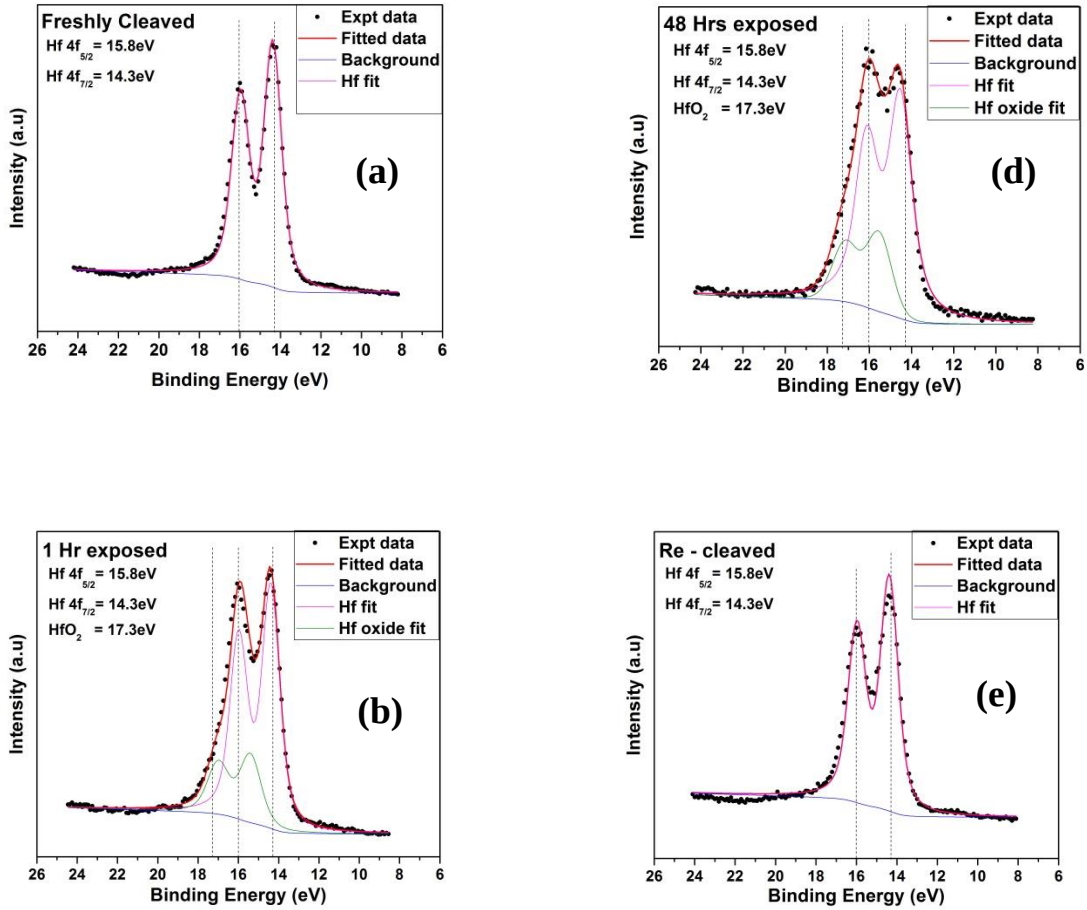

Figure 10 : Hf 4f peaks ; (a) Freshly cleaved $HfSe_2$ surface shows the Hf $4f_{5/2}$ and Hf $4f_{7/2}$ component peaks at binding energies of 14.3 eV and 16 eV, respectively. The peak profiles following ambient exposure of 1 hr (b), 3 hrs (c) and 48 hrs (d) clearly display the growth of higher binding energy oxide component peaks at 15.4 eV and 17.1 eV. The unoxidised Hf signal is regained after re-cleaving of the top surface, removing the surface oxide.

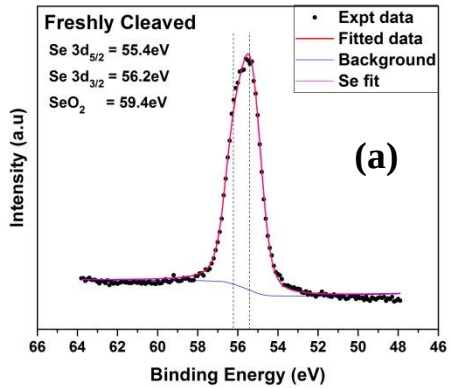

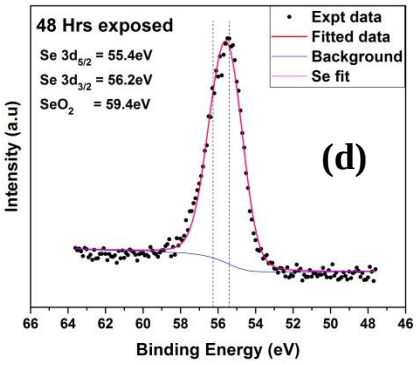

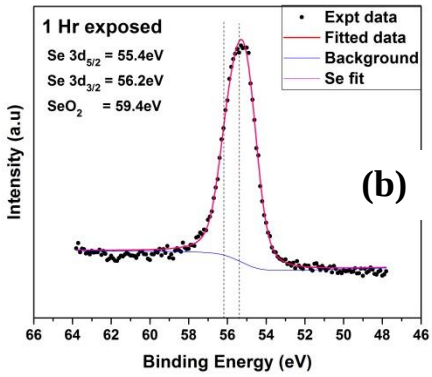

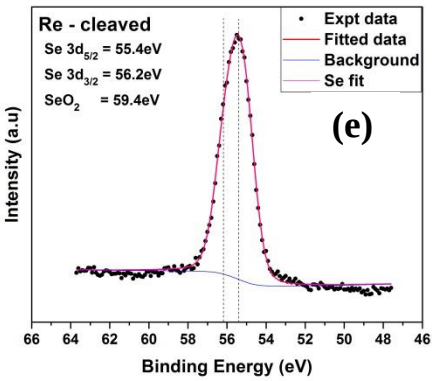

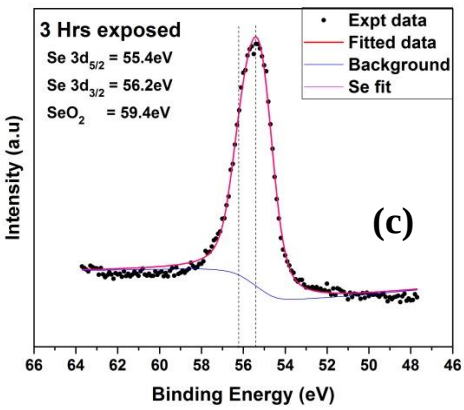

Figure 11 : Se 3d peaks ; (a) Freshly cleaved Se3d peak is curve fitted with an unresolved doublet with binding energy of Se 3d5/2=55.4 eV and Se 3d3/ = 56.4eV. Curve fits of the 1 hr (b), 3 hrs (c) and 48 Hrs (d) air exposed samples show no significant change to the peak profile with no evidence of higher oxidation states of selenium (e.g. SeO_2 which has a binding energy of 59.4eV). Recleaving the sample as shown in (e) leaves the peak profile unchanged.

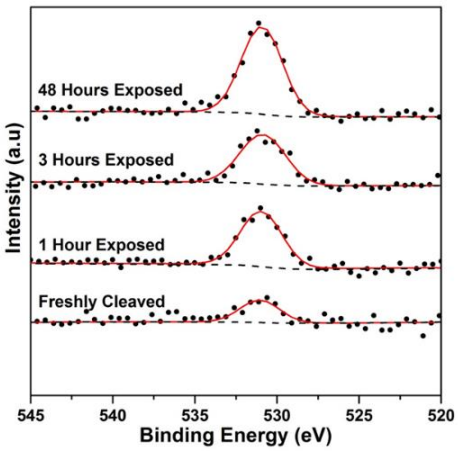

Figure 12: The O1s core level spectra as a function of exposure time

DISCUSSION

Even though $HfSe_2$ was the most reactive among the TMDs studied here, $HfSe_2$-based FETs are found in literature, with I_{on}-I_{off} ratio exceeding 7.5×10^6 reported by Kang et al.[13] These devices were quickly passivated with the resist PMMA, which can limit the effects of surface deterioration due to air exposure. In the supporting information of that work two AFM images of un-passivated $HfSe_2$ surface 1 and 8 days after exfoliation are reported, showing similar features to those presented in Fig. 2 in this work.

Also, a study of air exposure stability of $HfSe_2$ films grown by Molecular Beam Epitaxy (MBE) is reported by Yue et al.[14] The oxidation reactions are reported to be related to the top surface of the film, which is less prone to oxidation when the crystalline quality of the film is improved. A higher quality might also mean fewer discontinuities on the surface, like step-edges, which this study would suggest are the optimal sites for $HfSe_2$ surface degradation.

Very recently Gao et al.[15] showed that Chemical Vapour Deposition (CVD) grown monolayers of MoS_2 and WS_2 were very air sensitive. X-ray photoelectron and Auger electron spectroscopy performed in that work showed that gradual oxidation proceeded along grain boundaries along with the adsorption of organic contaminants. Degradation of CVD WS_2 was also reported by He et al.[16] Another promising 2D-material is Black Phosphorus, whose surface shows similar features[17,18,19] to that found for $HfSe_2$ here. The so-called bubbles grow in density and height after air exposure, regardless of the actual thickness of the Black Phosphorus flake, meaning that these effects are top-surface related. The density of these features on Black Phosphorus eventually decreases with air exposure since they become wider, merging together, but this behaviour was not in the current $HfSe_2$ study. In a subsequent study, Kim et al. reported the successful preparation of air stable multilayer

phosphorene thin-films and transistors.[20] In that work a double layer capping of Al_2O_3 and hydrophobic fluoropolymer was used to produce air stability of the material.

The surface roughness trends observed in our AFM data are in accordance with the DFT calculations carried out by Liu et al.[21] In that paper it was stated that a TMD is more easily converted to oxide as the chalcogen is varied from S, to Se, to Te, i.e. descending the periodic table. This can be due to the decrease in the electronegativity of the chalcogen from S to Te, resulting in the metal-chalcogen bond being more susceptible to oxidation. Moreover, that work restricts the interaction between oxygen and TMDs to single chalcogen vacancies. These defects are more likely to occur in more reactive TMDs, so, considering that the S vacancy density for MoS_2 is reported [22,23] to be in the order of 10^{13} cm^{-2}, the Se vacancy density would be expected to be higher in $HfSe_2$. Considering that defect density related to air exposure in this work is found to be in the order of 10^7 cm^{-2} from both the AFM and the SEM analysis, it is possible that these kind of features are not related to chalcogen vacancies alone. These defects could play a role in the overall process, [24, ,25] but not all of them appear to be optimal sites for the growth of the blister shaped protrusions.

It is clear that some of the TMD materials of interest from a device perspective are remarkably air sensitive.[26,27] Many other groups have reported material or electrical data indicating this, while the systematic study in this work gives more insight into the relative reactivity of the TMDs and form of the surface features. To think that these materials are purely 2D in nature is probably misleading, as this implies that top surface is totally unreactive in the perpendicular plane as there are no available covalent bonds in that plane. Unfortunately it is not that simple, as it is clear that molecules present in air react with the TMD surfaces. As stated above a surface encapsulation using resists, insulators, or dielectrics have been demonstrated elsewhere as being effective protection layers.

Other solutions may lie in the area of chemical functionalisation of surfaces. For example one might think of graphene as a perfectly 2D material with no free bonds available for surface reactions or functionalisation, however Long et al. found that graphene bonds non-covalently with alkane-amine groups,[28] providing a pathway for solution-phase self-assembly. Furthermore O'Connell et al.[29] discovered recently that molecular monolayer doping via chemisorption of organic molecules on Si surfaces actually supressed oxidation of the Si surface. In terms of surface protection of TMDs, non-covalent surface reactions or functionalisation may prove important to improving their air stability. Whatever the method, it is evident that air contact affects the structural and electrical properties of these TMD materials by various degrees. Tackling this issue is perhaps one of the biggest challenges for future TMD-based devices and technologies.

CONCLUSIONS

In this work we compared and contrasted the reactivity of MoS_2, $MoSe_2$, $MoTe_2$, HfS_2 and $HfSe_2$ in air. AFM, SEM, EDX, S-TEM, and XPS data were collected. Overall, surface roughening occurs for all TMDs over a period of time which indicates a formation of oxides or molecular adsorption on the surfaces. $HfSe_2$ and $MoTe_2$ were the most reactive of the TMDs studied. $HfSe_2$ in particular was characterised by the growth of Se-rich surface blisters, that form within one day of air exposure. It is theorised that the Hf is oxidising into HfO_2, which breaks down the $HfSe_2$ and excludes the Se at the surface. The Se atoms coalesce into blisters which continue to grow as more $HfSe_2$ is consumed and more HfO_2 is formed.

ACKNOWLEDGEMENTS

We acknowledge the support of Science Foundation Ireland through the US-Ireland R&D Partnership Programme "*Understanding the Nature of Interfaces in Two Dimensional*

Electronics (UNITE)" Grant Number SFI/13/US/I2862, and the support of the Irish Research Council through the Postgraduate Scholarship EPSPG/2015/69. The research was supported in part by the Higher Education Authority Programme for Research in Third Level Institutions in Ireland under Grant Agreement no. HEA PRTLI5.

REFERENCES

[1] H. Qiu, L. Pan, Z. Yao, J. Li, Y. Shi and X. Wang, Appl. Phys. Lett. 100, 123104 (2012);

[2] R. Addou, S. McDonnell, D. Barrera, Z. Guo, A. Azcatl, J. Wang, H. Zhu, C. L. Hinkle, M. Quevedo-Lopez, H. N Alshareef, L. Colombo, J. W. P. Hsu, R. M. Wallace, ACS Nano **9**, 9124 (2015).

[3] J. H. Kim, J. Lee, J. H. Kim, C. C. Hwang, C. Lee, J. Y. Park., Appl. Phys. Lett. **106**, 251606 (2015).

[4] R. Duffy, P. Foley, B. Filippone, G. Mirabelli, D. O'Connell, B. Sheehan, P. Carolan, M. Schmidt, K. Cherkaoui, R. Gatensby, T. Hallam, G. Duesberg, F. Crupi, R. Nagle, and P. K. Hurley, ECS Journal of Solid State Science and Technology **5**, Q3016 (2016).

[5] W. Park, J. Park, J. Jang, H. Lee, H. Jeong, K. Cho, S. Hong and T. Lee. Nanotechnology **24**, 095202 (2013).

[6] Q. Yue, Z. Z. Shao, S. L. Chang, and J. B. Li, Nanoscale Res. Lett. **8**, 425 (2013).

[7] S. Y. Lee, U. J. Kim, J. Chung, H. Nam, H. Y. Jeong, G. H. Han, H. Kim, H. M. Oh, H. Lee, H. Kim, Y. Roh, J. Kim, S. W. Hwang, Y. Park, and Y. H. Lee, ACS Nano **10**, 6100 (2016).

[8] K. S. Novoselov, A. K. Geim, S. V. Morozov, D. Jiang, Y. Zhang, S. V. Dubonos, I. V. Grigorieva, and A. A. Firsov, Science **306**, 666 (2004).

[9] J. Kim and K. Yong, J. Vac. Sci. Technol. B **24**, 1147 (2006).

[10] Moulder, J.F., Stickle, W.F., Sobol, P.E. and Bomben, K.D.., Handbook of X-ray Phototelectron Spectroscopy, Minnesota: Perkin-Elmer Corporation, 1992.

[11] Y. Liu, L. Si, X. Zhou, X. Liu, Y. Xu, J. Bao and Z. Dai, J. Mater. Chem. A **2**, 17735 (2014).

[12] J. Zhu, Y. R. Li, Z. G. Liu, J. Phys. D. Appl. Phys. 37 2896–2900 (2004).

[13] M. Kang, S. Rathi, I. Lee, D. Lim, J. Wang, L. Li, M. A. Khan, G.-H. Kim, Appl. Phys. Lett. **106**, 143108 (2015).

[14] R. Yue, A. T. Barton, H. Zhu, A. Azcatl, L. F. Pena, J. Wang, X. Peng, N. Lu, L. Cheng, Rafik Addou, S. McDonnell, L. Colombo, J. W. P. Hsu, J. Kim, M. J. Kim, R. M. Wallace, and C. L. Hinkle, ACS Nano **9**, 474 (2015).

[15] J. Gao, B. Li, J. Tan, P. Chow, T.-M. Lu, and N. Koratkar, ACS Nano **10**, 2628 (2016).

[16] Z. He, X. Wang, W. Xu, Y. Zhou, Y. Sheng, Y. Rong, J. M. Smith, and J. H. Warner, ACS Nano **10**, 5847 (2016).

[17] D. Wood, S. A. Wells, D. Jariwala, K. –S. Chen, E. Cho, V. K. Sangwan, X. Liu, L. J. Lauhon, T. J. Marks, and M. C. Hersam. Nano Letters **14**, 12 (2014).

[18] A. Castellanos-Gomez , L. Vicarelli, E. Prada, J. O. Island, K. L. Narasimha-Acharya, S. I. Blanter, D. J. Groenendijk, M. Buscema, G. A. Steele, 2D Mater. **1**, 025001 (2014).

[19] S. P. Koenig, R. A. Doganov, H. Schmidt, A. H. Castro Neto and B. Özyilmaz, Appl. Phys. Lett. **104**, 103106 (2014).

[20] J. –S. Kim, Y. Liu, W. Zhu, S. Kim, D. Wu, L. Tao, A. Dodabalapur, K. Lai and D. Akinwande, Scientific Reports **5**, 8989 (2015).

[21] H. Liu, N. Han, J. Zhao. RSC Adv. **5**, 17572 (2015).

[22] H. Qiu, T. Xu, Z. Wang, W. Ren, H. Nan, Z. Ni, Q. Chen, S. Yuan, F. Miao, F. Song, G. Long, Y. Shi, L. Sun, J. Wang, X. Wang. Nat. Commun. **4**, 2642 (2013).

[23] J. Hong, Z. Hu, M. Probert, K. Li, D. Lv, X. Yang, L. Gu, N. Mao, Q. Feng, L. Xie, J. Zhang, D. Wu, Z. Zhang, C. Jin, W. Ji, X. Zhang, J. Yuan and Z. Zhang , Nat. Comm. **6**, 6293 (2015).

[24] K. C. Santosh, R. C. Longo, R. M. Wallace, K. J. Cho, Appl. Phys. **117**, 135301 (2015).

[25] R. Addou, L. Colombo, R. M. Wallace, ACS Appl. Mater. Interfaces **7**, 11921 (2015).

[26] Y. Li, Z. Zhou, S. Zhang, Z. Chen, J. Am. Chem. Soc. **130**, 16739 (2008).

[27] G. Lee, X. Cui, D. Kim, G. Arefe, X. Zhang, C. Lee, F. Ye, W. Kenji, T. Taniguchi, P. Kim, J. Hone, ACS Nano, **9**, 7019 (2015).

[28] B. Long, M. Manning, M. Burke, B. N. Szafranek, G. Visimberga, D. Thompson, J. C. Greer, I. M. Povey, J. MacHale, G. Lejosne, D. Neumaier, and A. J. Quinn, Adv. Funct. Mater. **22**, 717 (2012).

[29] J. O'Connell, G. Collins, G. P. McGlacken, R. Duffy, and J. D. Holmes, ACS Materials and Interfaces **8**, 4101 (2016).